2014 IEEE/RSJ International Conference on
Intelligent Robots and Systems (IROS 2014)
September 14-18, 2014, Chicago, IL, USA

# Principles of Microscale Flexure Hinge Design for Enhanced Endurance

Ronit Malka*, Alexis Lussier Desbiens*, Yufeng Chen, and Robert J. Wood
*Contributed equally to the work

***Abstract*— Articulation based on flexure hinges is increasingly popular in microrobotics because of the absence of Coulomb friction, ease of manufacturability, fluid motion, durability, and large angular ranges. However, the inherent flexibility of these hinges makes modeling very complex and specific to the particular engineering applications for which they were developed. In this paper we describe the development and testing of a simplified, versatile method for modeling the stress on a flexure hinge under multi-axis loads in order to maximize hinge lifespan. We also discuss other stress concentration reducing features and design rules that can be applied to more general flexure hinge designs to further extend hinge lifespan.**

## I. Introduction

Flexure hinges, or living hinges, are common components in small-scale robots. Whereas articulation in larger scale robots has traditionally relied upon pin joints, bushings or bearings, the development of small *microrobots* requires new techniques to manufacture joints to overcome unfavorable friction scaling. Flexure hinges exhibit negligible friction, are compact and simple to manufacture using lamination and folding techniques such as the Smart Composite Microstructure (SCM) process [1], [2]. For these reasons, flexure hinges are a vital part in existing small biologically-inspired robotics, from running [3]–[5] to flying robots [6]. Flexure hinges have also been applied in many other engineering solutions, such as basic mechanisms [7], foldable robots [8], programmable matter [9] and medical devices [10].

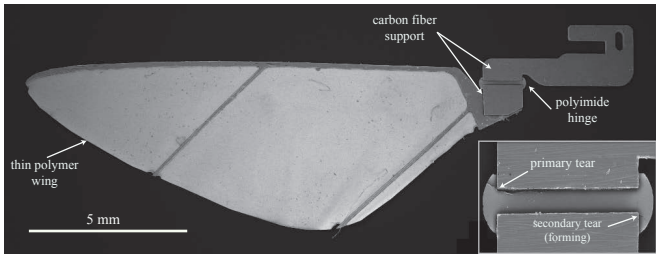


Fig. 1. RoboBee wing on a flexure hinge. The failure of the hinge initiates at the top corner of the hinge closest to the wing (top-left corner in this figure).

The wing hinge is especially important to the RoboBee [6]. As seen in Figure 1 wings are connected to the wing drive transmission with only thin strips of polyimide to mimic the efficient and passive vortex-capturing wing motion seen in nature [11], [12]. The RoboBee's wings flap at 100-120Hz, with a peak-to-peak angular deflection of $50$ to $100°$. Over time, the repeated motion of the wing causes fatigue failure of the hinges and requires delicate replacement of the hinge and recalibration of the bee for flight. This failure typically occurred in the RoboBee after approximately 10 minutes of flying, or 70,000 cycles. However, a much longer lifespan is thought to be possible with careful design, as polyimide can be cycled up to $10^7$ times when the applied stress is limited to 50 MPa [13]. From this, it seemed feasible to design longer-lasting hinges by better understanding the causes of their failure.

Understanding hinge failure, however, is a complicated task. Most publications on the subject predict the stiffness of all axes but only the stress experienced under simple loading conditions [14], [15]. Approximations of 3D hinge bending have also been developed [16]. Many models of flexure hinges have been developed for injection molded hinges with elliptical or circular cross sections [17], [18]. This work analyses the hinges used in the RoboBee and presents design rules for enhancing the lifespan of laminated flexure subject to complex, multi-axis loading.

## II. Hinge Design and Proposed Improvements

The RoboBee uses passive flexure hinges to generate pitch rotation during flapping. This process, inspired by the interplay of aerodynamic, inertial, and elastic forces that determine the motion of insect wings [12], reduces the number of actuators required to create the desired wing motion. A key parameter used to tune the motion of the wing is the stiffness of the hinge. For a hinge of width ($w$), length ($l$), and thickness ($t$), the rotational bending stiffness is defined as:

$$k = \frac{Et^3 w}{12L} \tag{1}$$

where $E$ is the Young's modulus of the material used [14], [15]. The Young's modulus is fixed by the material choice, while the geometry was previously chosen to create the bending stiffness required for passive rotation using the shortest length required to achieve the desired motion [19]. The present work attempts to minimize the stress sustained by the flexure hinge to maximize its lifespan.

### A. Hinge Manufacture and Design

The flexure hinges examined in this article were built with the SCM fabrication technique [1], using a polyimide film as the flexible hinge and carbon fiber as the stiff base and wing anchor. Individual layers of carbon fiber, polyimide

The authors are with the Harvard Microrobotics Laboratory, Harvard University, Cambridge, MA 02138, USA and the Mechanical Engineering Departement of the Université de Sherbrooke, Sherbrooke, Canada, J1K 2R1 {rmalka, yufengchen,rjwod}@seas.harvard.edu, Alexis.Lussier.Desbiens@USherbrooke.ca

film, and pyralux acrylic adhesive were laser cut with specific features necessary for hinge creation, then aligned and cured at 200°C for 2 hours under 350 kPa of pressure (Fig. 2). The cured assembly was then laser cut to release the hinges, which could then be attached separately to the wings and wing driver transmission. Two types of hinges were used for testing: hinges that are the same dimensions as the RoboBee hinges (1.25mm wide x 70μm long x 7.5μm thick), and short-lived hinges (lasting about 5 minutes) used for rapid lifespan testing (1.45mm wide x 125μm long x 12.7μm thick).

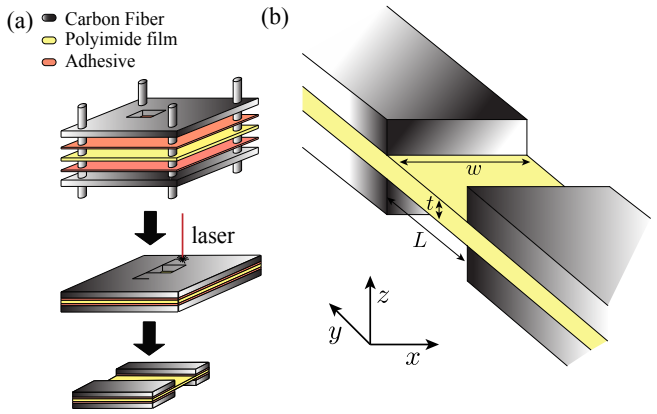


Fig. 2. Creating a laminate of carbon fiber, polyimide and adhesive as part of the SCM fabrication of a flexure hinge (left). Hinge dimensions and coordinate frame used (right). The $x$-axis points toward the wing tip while the $y$-axis points toward the top of the bee.

In this fabrication process, carbon fiber was selected as the structural element because of its high specific stiffness. Although materials like polyethylene and polypropylene have traditionally been used in living hinges due to their fatigue resistance and compatibility with injection molding, they are not compatible with the high temperature involved in the fabrication of these laminates. Instead, polyimide is chosen for both its thermal and mechanical properties, available under the trade name Kapton in thicknesses of 7.5, 12.7 and 25μm.

### B. Proposed stress concentration reducing features

One hypothesis to explain the short lifespan of the standard wing hinge is that the failure is caused by a stress concentration at the corners of the hinge, where the carbon fiber and the polyimide meet. Stress concentration, a localized increased in stress magnitude, typically happens due to a geometric change in section, a crack, a sharp corner, or a change in material stiffness. To reduce potential stress concentrations, various stress-reduction features have been used on the RoboBee. Three of these features are illustrated in Figure 3, along with the standard design, and their effects on hinge lifespan were tested as part of this work. The rounded corner feature was developed to remove the sharp corners where the primary tear typically forms. The stress relief feature increases the amount of polyimide around the stress concentration, so cracks take longer to expand into tears that cause hinge failure. The adhesive support feature was developed to increase the off-axis torsional stiffness with minimal effect on the bending. Other ideas include adhesive support that had the two strips of adhesive left on the top and bottom edges of the hinge rather than the side edges (morphologically similar to stress relief features common on electrical cables), but this feature was difficult to fabricate due to the required alignment tolerances.

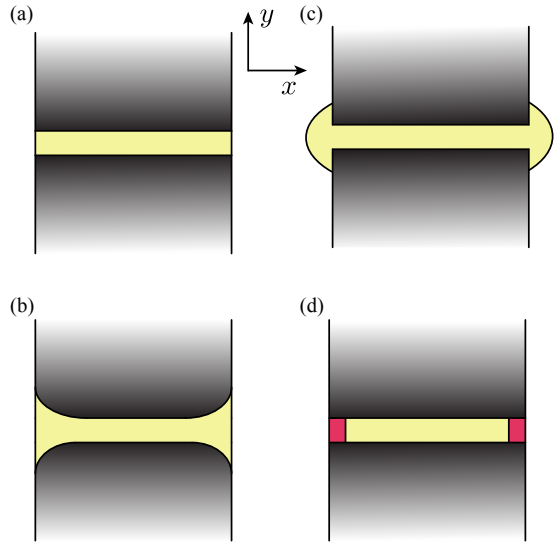


Fig. 3. Diagram of different stress concentration reducing features, labelled: (a) plain hinge, (b) rounded corner, (c) stress relief, (d) vertical adhesive support. Features are exaggerated here to better demonstrate their design.

### C. Hinge sizing for reduced stress

A desired hinge stiffness, as described by Equation (1), can be achieved by altering the material choice or flexure geometry. To guide the designer during hinge design, a model of beam bending under pure moment, and thus constant bending radius, was first used. If we assume a hinge bending angle of $\theta$ and a radius R to the center of the circle defined by the bending hinge, we can express the length of the neutral axis $L_N$ as $\theta R$ and the length of the stretched outer surface $L_E$ as $\theta(R + \frac{t}{2})$. From this, we find:

$$\Delta L = L_E - L_N = \theta\left(R + \frac{t}{2}\right) - \theta R = \frac{\theta t}{2} \qquad (2)$$

Thus, since $\sigma = E\epsilon$, we find the hinge stress calculated using constant curvature, expressed by the equation:

$$\sigma = \frac{E\theta t}{2L_N} \qquad (3)$$

For the RoboBee's wing hinges, the pitch angle is defined by the interplay of aerodynamic and inertial forces on the wing and the elastic torque of the flexure. Though the maximal lift is achieved with a hinge amplitude of 45°, the

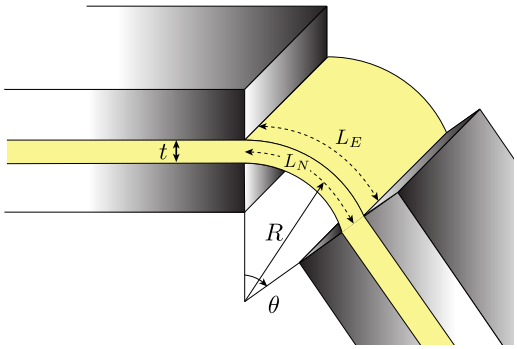


Fig. 4. Cross-section of bending hinge with thickness t, neutral length $L_N$, edge length $L_E$, radius R, and hinge angle $\theta$.

robot's wings are flapped at a mean hinge amplitude of 35°. The margin of extra lift at large hinge amplitude is reserved for flight stability control. Looking at Equation (1) and (3), different geometric combinations can be used to minimize the stress in the hinge while maintaining a constant stiffness:

*1) Varying width and length:* Increasing $w$ and $L$ by a factor of $a$ doesn't affect the stiffness of the hinge, but multiplies the stress by a factor of $1/a$ due to the increase in $L$.

*2) Varying thickness and length:* Increasing hinge thickness by a factor of $a$ requires a corresponding increase of the length by a factor of $a^3$ to maintain a constant stiffness. This multiplies the stress by a factor of $1/a^2$.

*3) Varying Young's modulus:* Increasing the Young's modulus by a factor of $a$ requires a corresponding change in $t^3w/L$ to maintain the stiffness. A change in $w$ will multiply the stress by a factor of $a$, while a $1/a$ change in $L$ will keep the stress constant. At best, increasing $E$ by $a$, with a corresponding $(1/a)^{1/3}$ change in the thickness, will multiply the stress by a factor of $a^{2/3}$. Lower values of $E$ are thus recommended, as long as the ultimate strength ($\sigma_u$) of the replacement material can be maintained.

Unfortunately, only certain thickness of polyimide film are available (i.e., 7.5, 12.7 and 25$\mu$m) and increasing the film thickness to 12.7$\mu$m led to oversized hinges that did not fit well the RoboBee design. Materials with lower Young's modulus do exist (e.g., rubber, silicone, urethane), but many can't survive the lamination temperature and are difficult to source in thin films. Thus, this paper focuses only on varying the width to length ratio to reduce the stress and increase the lifespan of the hinge.

Modifying the dimensions of the flexure hinge also impacts the off-axis stiffnesses. Fortunately, the impact on the off-axis stiffnesses is minimal when increasing both the width and length of the flexure by a factor of $a$ as proposed. Using the off-axis stiffness equations described in [15], one can see that both the linear stiffness along the $y$-axis and the revolute stiffness around the $y$-axis remain effectively unchanged. On the other hand, the revolute stiffness around the $z$-axis increases by a factor of $a^2$ while the linear stiffness along the $z$-axis is multiplied by a factor of $1/a^2$. For the dimension used in this work, this reduction in linear stiffness has little impact on the motion of the wing. Finally, when modeled as a clamped-free column, the maximum compressive load that the flexure can sustain prior to buckling is multiplied by a factor of $1/a$. However, buckling hasn't been observed for the hinge dimensions and loads used in this work.

## III. Finite Element Analysis Modeling

The constant bending radius model assumes that the hinges are loaded with a pure bending moment around the $x$-axis. This model neglects the off-axis loading and suggests the presence of a constant stress at the surface of the hinges. Although this model is helpful to guide the sizing of the hinge, it doesn't predict the contribution of the off-axis loading to the hinge stress and doesn't explain why the failures initiate only from the top corner of the hinge closest to the wing. As direct stress measurements are difficult, a finite element model was developed in COMSOL to better understand the stress experienced by the hinge under the loads created by flapping. The hinge was modeled as a rectangular prism with a Young modulus of 2.5GPa, a Poisson's ratio of 0.34, and a density of 1420kg/m$^3$ [20]. One end of the hinge is fixed while a rigid connector applies representative forces and moments at the other end.

Both the inertial and aerodynamical forces play an important role in the motion of the Robobee wing and in the stress experienced by the hinge. The amplitude of the aerodynamical forces and the chordwise inertial force are both maximum at midstroke, while the spanwise inertial force is maximum at stroke reversal. However, for the wing geometry, the wing mass distribution and the flapping motion used by the Robobee, the bending moments created at the hinge by the inertial forces through the full motion are ten times smaller than the bending moments created by the aerodynamical forces at midstroke. For this reason, the finite element analysis presented in this paper focuses on the hinge behavior at midstroke and ignores the inertial forces. The following sections describe the calculation of the aerodynamical forces at midstroke and describe the results obtained by the finite element analysis.

### A. Aerodynamical Forces Modeling

The aerodynamical forces and moments acting on the hinge at midstroke can be approximated by using the quasi-steady model proposed in [21]. According to this model, the lift and drag forces acting on the wing surface are computed by integrating along the spanwise direction $\hat{r}$:

$$F_L = \frac{1}{2} C_L(\alpha) \rho \int_{x_r}^{x_r+R} (2\pi f \phi_m r)^2 c(r) dr \qquad (4)$$

$$F_D = \frac{1}{2} C_D(\alpha) \rho \int_{x_r}^{x_r+R} (2\pi f \phi_m r)^2 c(r) dr \qquad (5)$$

where $C_L$ and $C_D$ are lift and drag coefficients, $\rho$ is the density of air, $f$ is the flapping frequency, $\phi_m$ is the stroke amplitude, $\alpha = \pi/2 - \psi$ is the angle of attack and $c$ is the

local chord length. Figure 5 illustrates the definition of the coordinate systems and also direction of lift and drag forces.

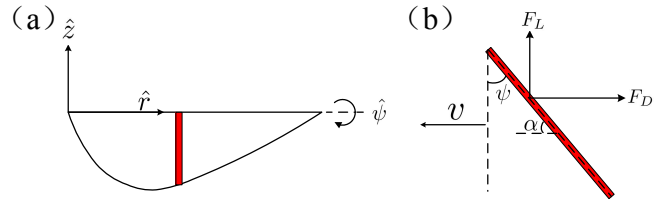


Fig. 5. Coordinate definitions of the quasisteady aerodynamic model. (a) shows the vertical $\hat{z}$ axis and spanwise axis $\hat{r}$. The rotation with respect to the wing hinge line gives the hinge motion. The quasisteadey model sums instantaneous force on every wing chord colored in red. (b) shows the definition of lift and drag forces on a single wing chord. Lift always points in the vertical axis and drag is opposite to the wing translational velocity. Angle of attack $\alpha$ is related to hinge angle $\psi$

We can further estimate the aerodynamic torque by computing the integral:

$$\bar{\Gamma} = \int_{x_r}^{x_r+R} \bar{r} \times d\bar{F} \tag{6}$$

In particular, the $\hat{z}$ component and $\hat{\psi}$ component are given by

$$\Gamma_\psi = \frac{1}{2}\left(C_L\cos(\alpha) + C_D\sin(\alpha)\right) \times ... \int_{x_r}^{x_r+R} (2\pi f \phi_m r)^2 c(r)\left(y_{LE}(r) - c(r) r_{cop}(\alpha)\right) dr \tag{7}$$

$$\Gamma_z = \frac{1}{2} C_D \sin\alpha \int_{x_r}^{x_r+R} (2\pi f \phi_m r)^2 c(r)\left(x_r + r\right) dr \tag{8}$$

where $(y_{LE}(r) - c(r) r_{cop}(\alpha))$ is the local chordwise center of pressure. The non-dimensionalized center of pressure ratio $r_{cop}(\alpha)$, lift coefficient $C_L(\alpha)$, and drag coefficient $C_D(\alpha)$ are taken from Dickinson's previous study [21].

Having estimated the aerodynamic torque, we can obtain the center of pressure in the wing coordinate as:

$$R_{cop} = \frac{\Gamma_z}{F_D} \tag{9}$$

$$Y_{cop} = \frac{\Gamma_\psi}{F_L\cos\alpha + F_D\sin\alpha} \tag{10}$$

For $\alpha$ = 55° and the wing shape used on the RoboBee, $F_L = 5.86\times10^{-4}$N, $F_D = 8.31\times10^{-4}$N, $R_{cop} = 8.7$mm and $Y_{cop} = -1.1$mm. To calculate the moment applied at the end of the hinge as a function of its pitch angle, the hinge is assumed to bend at its halfway point as suggested by [14]. This results in the following moment at the end of the hinge:

$$M_x = \left(-\frac{L}{2} - \left(Y_{cop} - \frac{L}{2}\right)\cos\theta\right) F_D + ... \left(Y_{cop} - \frac{L}{2}\right)\sin\theta F_L \tag{11}$$

$$M_y = -R_{cop} F_D \tag{12}$$

$$M_z = R_{cop} F_L \tag{13}$$

### B. Finite Element Analysis Validation and Results

To validate the COMSOL FEA model, hinges with stiffnesses equal to that in the RoboBee hinge ($1.57\times10^{-6}$Nm/rad) and lengths between 60 and 240μm were subjected to a pure moment $M_x$. The maximum stress found was compared to Equation (3). The results are illustrated in Figure 6 and agree within a few megapascals. These solutions were obtained with a mesh of 56,000 elements, after varying the total number of elements from 5,000 to 247,000.

The calculated angular deflection of these hinges around the $x$-axis under the full aerodynamics load described previously correspond to the values observed experimentally (i.e., 35.5°). As expected from the off-axis stiffnesses [15], the angular displacement around the $y$-axis remains constant at 0.9° while the angular displacement around the $z$-axis decreases with increasing hinge length. Fortunately, the angular displacement around the $z$-axis is small even for short hinges (i.e., $5\times10^{-3}$ degree for $L = 60\mu$m).

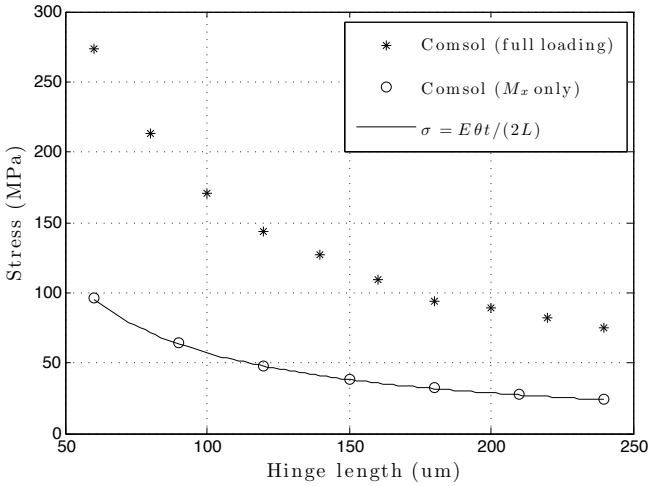


Fig. 6. Validation of FEA model against beam bending under pure $M_x$ moment and effect of off-axis aerodynamical loads on the hinge. Off-axis aerodynamical loads cause stress almost three times higher than expected.

As illustrated in Figure 6, both the maximum stress experienced under the full aerodynamical load, described in Section III, and the maximum stress sustained under a pure bending moment $M_x$ decrease with increasing hinge length. However, the maximum stress experienced by the hinge under the full aerodynamical loading is almost three times higher than expected under a pure $M_x$ bending moment. Furthermore, it appears that the hinges used on the RoboBee ($w = 70\mu$m) operate close to the ultimate strength of the polyimide material used ($\sigma_u = 231$MPa). One can also notice that a small increase in the length of the hinge from 70 to 100μm rapidly reduces the maximum stress from 230 to 170MPa.

Finally, as illustrated in Figure 7, the highest stress experienced under realistic loading conditions is located at the top edge of the hinge near the wing (top-right corner) - the same corner where the primary tears formed on each hinge that failed.

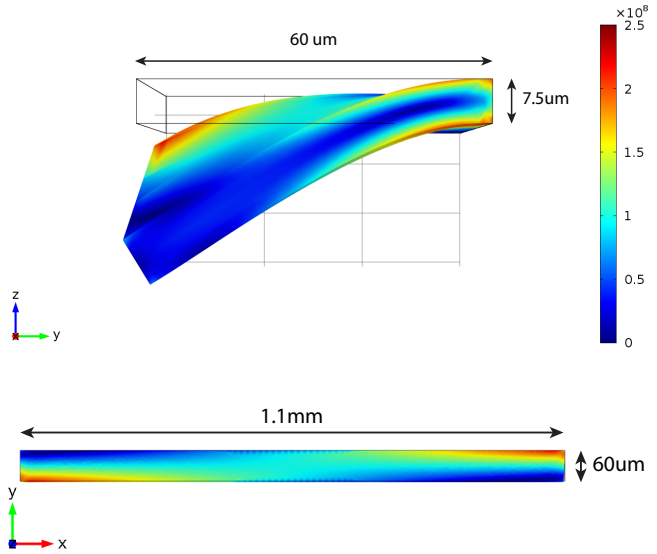


Fig. 7. View along the rotational axis of a hinge (top figure) of the displacement and stress, illustrated by the color scale (units in Pascals) under the full aerodynamical load. Bottom figure shows a view of the same hinge, this time with the thickness axis oriented out of the page. The maximum stress from this simulation, in the top-right corner of the bottom figure, is located in the same corner as where the failures initiate experimentally.

## IV. Experimental Setup

A chamber specially designed for flapping-wing experiments was used to evaluate both stress concentration reducing features and the effect of hinge sizing. The important components of this chamber are described in the following sections.

### A. Wing Driver and Force Sensor

Wings are flapped using the wing driver shown in Figure 8. This mechanism converts the tip motion of a bimorph piezoelectric actuator into the single degree of freedom wing stroke. Due to the inertial and aerodynamic forces generated, passive rotation occurs about the flexure hinge connecting the wing to the driver.

The wing driver was installed on the input plate of a two axis force sensor [22]. This sensor is made of a single sheet of 150$\mu$m Invar that is folded and welded into four parallel dual cantilevers, 4x4x7mm each. These beams are arranged in a series-parallel configuration to convert loads transmitted through the input plate into orthogonal displacements along the $y$ (vertical) and $z$ axes (horizontal). Both $y$ and $z$ axes have a sensitivity of approximately 85V/N and a resonant frequency of 510Hz. Force signals were digitized at 5kHz.

More details about the wing driver and the force sensor can be found in [23], [24].

### B. Failure Detection

As described previously, failure starts at the top corner of the hinge closest to the wing. A crack propagates over the entire length of the hinge within 500-1000 flapping cycles, eventually causing complete detachment of the wing from the hinge. As the crack propagates, the wing motion changes considerably leading to collision of the top and bottom part of the hinge. This results in a characteristic increases in the horizontal force acting on the wing at the start of failure (Fig. 9). This spike in force was detected by comparing the instantaneous value of the horizontal force to the maximum force recorded during the first five seconds of the test. When the instantaneous horizontal force became 1.5 times greater than the initial drag readings, the hinge was considered broken and the test was terminated.

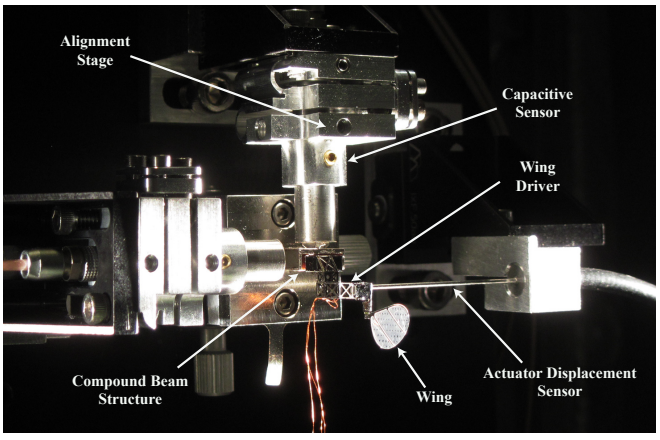


Fig. 8. Wing driver assembly (from [23])

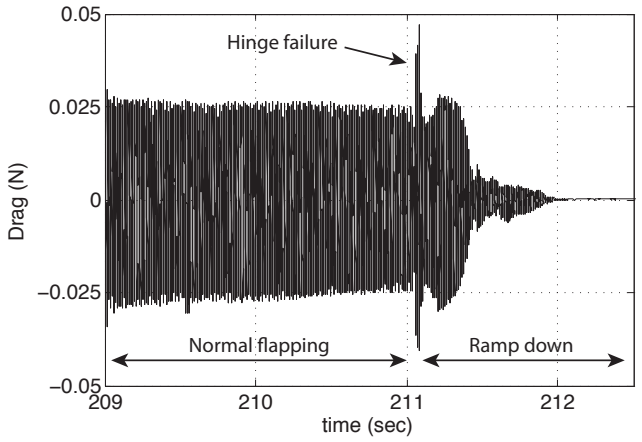


Fig. 9. Typical horizontal force recorded during the last few seconds of flapping. This figure shows normal flapping and the spike in force caused during hinge failure. The control software detects the failure and slowly reduces the flapping amplitude to a complete stop before complete detachment of the wing from the hinge can happen.

### C. Pitch and Stroke Angle Determination

The motion of the wing was recorded during six cycles of flapping with a Phantom V7.3 camera equipped with an AF MICRO Nikkor 200mm f/4 lens positioned normal to the stroke plane. The resulting 10kHz video was post-processed to extract the pitch (i.e., hinge angle) and stroke angles of the wing. To do so, the wing area projected onto the image frame and its major axes were extracted from each frame. This information was combined with the known position of

the wing driver joints and the aspect ratio of the wing to extract the motion of the wing as described in [23].

## V. Results

### A. Stress Concentration Reducing Features

The stress concentration reducing features were tested on the shorter-lived hinges and on a wing design slightly different than what is used on the RoboBee. This wing has an aspect ratio of three and second moment of area of 0.55, as presented in [23], and uses stiffer hinges (1.45mm x 125μm x 12.7μm) at a frequency of 160Hz. This wing was used for initial testing of hinge alterations because the short-lifespan hinges would allow us to more quickly determine the relative effect of the different hinge designs. The results of the rounded corner and stress relief features in affecting hinge lifespan are shown in Figure 10a. For this test, eight to nine hinges were flapped until failure for each model. None of these features appeared to have a statistically significant effect on lifespan. Figure 10b shows the results of another hinge test comparing different adhesive support: horizontal strips, vertical strips and stress relief features made of the adhesive layer (three hinges per model). Hinges were flapped until failure for each model. From our results, all forms of adhesive support had a negligible effect on lifespan. However, the acrylic adhesive used in our manufacturing process is very pliable and might not provide enough support to counteract the hinge torsion. Using another, stiffer material might have led to a more significant result.

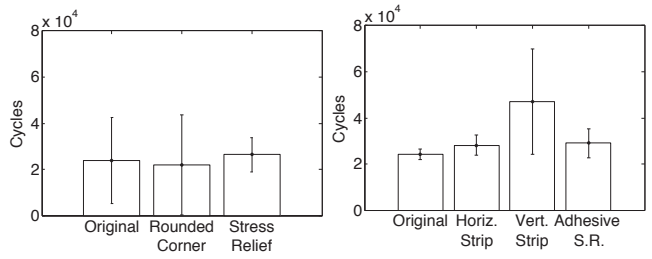


Fig. 10. All hinges tested were short-lived hinges used for rapid testing and prototyping (1.45mm wide x 125μm long x 12.7μm thick). (left) Rounded corner and stress relief features showing negligible effects on lifespan compared to the standard hinges. The error bars show one standard deviation, which in some cases is of similar magnitude as the hinge lifespan. A total of 8 hinges were tested for the original and stress relief features, and 9 for the rounded corner features. (right) Vertical adhesive support (each 100 μm wide), horizontal adhesive support (each 15 μm tall), and stress relief made from adhesive, also showing negligible lifespan enhancement compared to the standard hinges. Two hinges were tested for the original feature, and 3 hinges for each of the horizontal strip, vertical strip, and adhesive stress relief features.

It is important to note that the hinges used to obtain each graph in Figure 10 come from different production runs. Due to manufacturing variation these test can't be compared to each other directly. That is why each production run includes a control model (i.e., the original hinge).

These results show stress-reducing features have virtually no effect in extending hinge lifespan, suggesting the hinge failure is not due to a stress concentration caused by the change in stiffness at the carbon-polyimide interface or the sharp corners of the hinge.

### B. Hinge Sizing for Stress Reduction

As described earlier, longer hinges experience reduced stress for a given hinge bending motion, thickness, and Young's modulus. Furthermore, the hinge stiffness can be maintained by increasing the hinge width by the same factor. To validate the effectiveness of this scaling technique to increase the hinge lifespan, a hinge 30% longer and wider than the short-lived protyping hinge was tested against hinges with other stress-reducing features. The increased lifespan of this new hinge is compared to the effect of the stress concentration reduction features in Figure 11. This 30% increase in the hinge length and width results in a 13× increase in its lifespan, without noticeably affecting its motion.

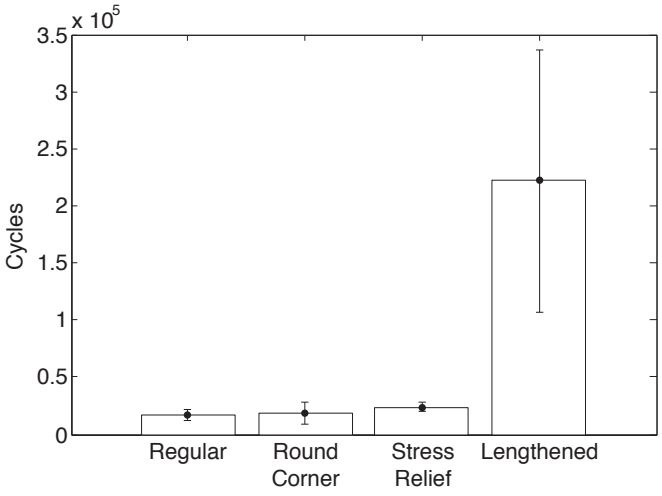


Fig. 11. Hinge lifespan of standard flexure hinges, hinges with rounded corners, hinges with stress relief, and regular hinges lengthened by 30 percent. Lengthening the hinge significantly increases the lifespan of the hinge. Error bars indicate one standard deviation. Three hinges were tested for all groups, and all hinges tested in this preliminary study were short-lived hinges for rapid testing and prototyping.

To further quantify how hinge length affects flexure hinge life, hinges with lengths varying from 55μm to 105μm were tested until failure in the wing testing chamber described above. Three hinges of each length were tested, and averages of the number of cycles withstood for each hinge length were found and plotted against length (Fig. 12). This data demonstrates that hinge lifespan is a function of length. The collected data fit with an exponential curve ($R^2$ = 0.87) where the lifespan increases with the length of the hinge. Although some materials like steel reach an infinite lifespan at a certain stress level, many polymers exhibit an exponential curve similar to the one observed in this work.

Hinges longer than 105μm were not tested as they lasted multiple hours. This is more than sufficient for the current RoboBee and also requires long tests on a shared instrument. It is believed that further increase of the hinge length will continue to increase their lifespan, up to a point where

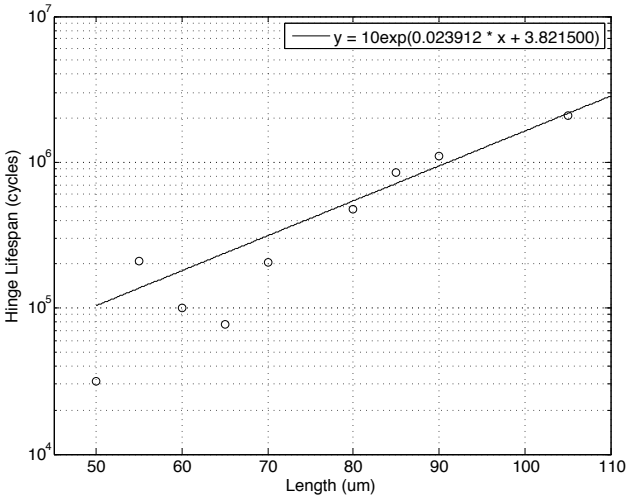


Fig. 12. Hinge lifespan as a function of length for hinges of constant revolute stiffness but varying length. This graph demonstrates the correlation between hinge length and lifespan, as predicted by equation 3. For each length, 3 hinges were tested using the longer-lived RoboBee hinge.

off-axis stiffness and flapping motion will be significantly affected.

Although all hinges were designed to have the same stiffness, wing motion was extracted to confirm that the resulting flapping motion was not affected by the dimensional change of the hinges or manufacturing variations. Little difference was found in hinge ($34\pm1.4°$) and stroke ($29.6\pm1.2°$) angles of all the hinges used in the experiments. This confirms that the off-axis stiffnesses were not affected by the change in width and length, or remained high enough to sustain the loads created by flapping.

## VI. Conclusion

This paper explored the failure mode of the compliant hinges used as the passive pitch joint of the RoboBee wing. These flexure hinges, consisting of a laminate of carbon fiber composites and thin polyimide film typically last approximately 10 minutes. Various methods were proposed to reduce the stress sustained by the hinge during normal flapping while keeping the stiffness - a characteristic critical to proper passive wing rotation - constant. Using experimental techniques, simple beam bending modeling and FEA, it was determined that (1) high stress at the corners of the hinge were not due to the sharp corners or stiffness transition, (2) off-axis loads contributed significantly to the total stress experienced by the hinge, and (3) increasing length and width substantially reduced the stress in the hinge without noticeable impact on the wing motion.

The experiments further revealed that slight modification to the dimensions can easily increase the lifespan of these hinges from a few minutes (70,000 cycles) to several hours (2,000,000+ cycles). Although material selection or thickness could still lead to improvements, longer polyimide hinges are currently being implemented into the newly fabricated RoboBees. More generally, the simple design rule detailed in this paper should prove useful to anyone designing multi-layer flexure-based mechanisms.

## References


[1] R. Wood, S. Avadhanula, R. Sahai, E. Steltz, and R. Fearing, "Microrobot design using fiber reinforced composites," *Journal of Mechanical Design*, vol. 130, p. 052304, 2008.

[2] J. Whitney, P. Sreetharan, K. Ma, and R. Wood, "Pop-up book mems," *Journal of Micromechanics and Microengineering*, vol. 21, no. 11, p. 115021, 2011.

[3] A. Baisch, O. Ozcan, B. Goldberg, D. Ithier, and R. Wood, "High speed locomotion for a quadrupedal microrobot," *International Journal of Robotics Research*, In Press.

[4] P. Birkmeyer, K. Peterson, and R. S. Fearing, "Dash: A dynamic 16g hexapedal robot," in *Intelligent Robots and Systems, 2009. IROS 2009. IEEE/RSJ International Conference on*. IEEE, 2009, pp. 2683–2689.

[5] A. M. Hoover, S. Burden, X.-Y. Fu, S. S. Sastry, and R. S. Fearing, "Bio-inspired design and dynamic maneuverability of a minimally actuated six-legged robot," in *Biomedical Robotics and Biomechatronics (BioRob), 2010 3rd IEEE RAS and EMBS International Conference on*. IEEE, 2010, pp. 869–876.

[6] K. Y. Ma, P. Chirarattananon, S. B. Fuller, and R. J. Wood, "Controlled flight of a biologically inspired, insect-scale robot," *Science*, vol. 340, no. 6132, pp. 603–607, 2013.

[7] J. O. Jacobsen, B. G. Winder, L. L. Howell, and S. P. Magleby, "Lamina emergent mechanisms and their basic elements." ASME, 2010.

[8] S. M. Felton, M. T. Tolley, B. Shin, C. D. Onal, E. D. Demaine, D. Rus, and R. Wood, "Self-folding with shape memory composites," *Soft Matter*, 2013.

[9] E. Hawkes, B. An, N. Benbernou, H. Tanaka, S. Kim, E. Demaine, D. Rus, and R. Wood, "Programmable matter by folding," *Proceedings of the National Academy of Sciences*, vol. 107, no. 28, pp. 12 441–12 445, 2010.

[10] J. Gafford, S. Kesner, R. Wood, and C. Walsh, "Microsurgical devices by pop-up book mems," *ASME/IDETC: Robotics and Mechanisms in Medicine*, 2013.

[11] S. P. Sane, "The aerodynamics of insect flight," *The journal of experimental biology*, vol. 206, no. 23, pp. 4191–4208, 2003.

[12] A. J. Bergou, S. Xu, and Z. Wang, "Passive wing pitch reversal in insect flight," *Journal of Fluid Mechanics*, vol. 591, no. 1, pp. 321–337, 2007.

[13] W. Glaeser, *Materials for tribology*. Access Online via Elsevier, 1992, vol. 20.

[14] L. L. Howell, *Compliant mechanisms*. Wiley-Interscience, 2001.

[15] M. Goldfarb and J. E. Speich, "A well-behaved revolute flexure joint for compliant mechanism design," *Journal of Mechanical Design*, vol. 121, p. 424, 1999.

[16] L. U. Odhner and A. M. Dollar, "Toward simpler models of bending sheet joints," in *Intelligent Robots and Systems (IROS), 2011 IEEE/RSJ International Conference on*. IEEE, 2011, pp. 1420–1426.

[17] S. T. Smith, V. G. Badami, J. S. Dale, and Y. Xu, "Elliptical flexure hinges," *Review of Scientific Instruments*, vol. 68, no. 3, pp. 1474–1483, 1997.

[18] N. Lobontiu, *Compliant mechanisms: design of flexure hinges*. CRC press, 2003.

[19] R. J. Wood, "Design, fabrication, and analysis of a 3dof, 3cm flapping-wing mav," in *Intelligent Robots and Systems, 2007. IROS 2007. IEEE/RSJ International Conference on*. IEEE, 2007, pp. 1576–1581.

[20] Dupont, "Summary of properties for kapton polyimide films," online, 2014.

[21] M. H. Dickinson, F.-O. Lehmann, and S. P. Sane, "Wing rotation and the aerodynamic basis of insect flight," *Science*, vol. 284, no. 5422, pp. 1954–1960, 1999.

[22] R. J. Wood, K. Cho, and K. Hoffman, "A novel multi-axis force sensor for microrobotics applications," *Smart materials and structures*, vol. 18, no. 12, p. 125002, 2009.

[23] A. Lussier Desbiens, Y. Chen, and R. J. Wood, "A wing characterization method for flapping-wing robotic insects," in *Intelligent Robots and Systems (IROS), 2013 IEEE/RSJ International Conference on*. IEEE, 2013, pp. 1367–1373.

[24] J. P. Whitney, "Design and performance of insect-scale flapping-wing vehicles," Ph.D. dissertation, Harvard University, 2012.